Unique and remarkable dilatometer measurements of pyroclastic flow–generated tsunamis

G.S. Mattioli   University of Arkansas, Fayetteville, Arkansas 72701, USA
B. Voight   Pennsylvania State University, University Park, Pennsylvania 16802, USA
A.T. Linde ⎤
I.S. Sacks ⎦ Carnegie Institution of Washington, 530 P Street NW, Washington, D.C. 20005, USA
P. Watts   Applied Fluids Engineering, Inc., 5710 E 7th St. #237, Long Beach, California 90803, USA
C. Widiwijayanti ⎤
S.R. Young ⎟
D. Hidayat ⎥ Pennsylvania State University, University Park, Pennsylvania 16802, USA
D. Elsworth ⎦
P.E. Malin ⎤
E. Shalev ⎦ Duke University, Durham, North Carolina 27708, USA
E. Van Boskirk ⎤
W. Johnston ⎦ University of Arkansas, Fayetteville, Arkansas 72701, USA
R.S.J. Sparks   University of Bristol, Tyndall Avenue, Bristol BS8 1TH, UK
J. Neuberg   University of Leeds, Leeds LS2 9JT, UK
V. Bass ⎤
P. Dunkley ⎟
R. Herd ⎥
T. Syers ⎥ Montserrat Volcano Observatory, Salem, Montserrat, West Indies
P. Williams ⎥
D. Williams ⎦

ABSTRACT

Pyroclastic flows entering the sea may cause tsunamis at coastal volcanoes worldwide, but geophysically monitored field occurrences are rare. We document the process of tsunami generation during a prolonged gigantic collapse of the Soufrière Hills volcano lava dome on Montserrat on 12–13 July 2003. Tsunamis were initiated by large-volume pyroclastic flows entering the ocean. We reconstruct the collapse from seismic records and report unique and remarkable borehole dilatometer observations, which recorded clearly the passage of wave packets at periods of 250–500 s over several hours. Strain signals are consistent in period and amplitude with water loading from passing tsunamis; each wave packet can be correlated with individual pyroclastic flow packages recorded by seismic data, proving that multiple tsunamis were initiated by pyroclastic flows. Any volcano within a few kilometers of water and capable of generating hot pyroclastic flows or cold debris flows with volumes greater than 5×10^6 m³ may generate significant and possibly damaging tsunamis during future eruptions.

Keywords: pyroclastic flows, tsunamis, volcanoes, Soufrière, Montserrat.

INTRODUCTION

The Soufrière Hills volcano on Montserrat began its current eruption in July 1995 (Druitt and Kokelaar, 2002), and produced its largest dome collapse on 12 July 2003 (Herd et al., 2005), which at $\sim 210 \times 10^6$ m³ is the largest to occur historically. This massive collapse and eruption was recorded on three CALIPSO Project (Mattioli et al., 2004) borehole dilatometers (TRNT, AIRS, and GERD), two borehole seismometers (TRNT, AIRS), several continuous global positioning system (cGPS) sites, and also by a surface broadband seismometer and acoustic microphone at HARR (locations shown in Fig. 1).

Important observations on the collapse include (all times UTC) a rainstorm between 11:00 and 13:00 on 12 July 2003 synchronous with the onset of small pyroclastic flows (PFs), which built in intensity through the day (Herd et al., 2005); large PFs after 22:00, which reached the seashore at Tar River Fan (TRF, ~3 km from the dome summit; Fig. 1), generating phreatic explosions; and pyroclastic surges, which reached 2–3 km offshore after 00:00 13 July 2003 (Edmonds and Herd, 2005), suggesting that dense basal layers of the PFs were entering the sea.

Eyewitness observations are correlated with the seismic signals generated by individual PFs. The peak seismic intensity, representing a major collapse, occurred around 03:30. Radio transmission from White's Yard (Fig. 1) was terminated at 03:36 by a surge cloud from the largest collapse. The 03:30 collapse unroofed the conduit, causing a short-lived Vulcanian explosion at 03:35. Thereafter, dome collapse waned and ended by ~07:00 on 13 July (Herd et al., 2005).

TSUNAMI RUNUP OBSERVATIONS

While tsunamis have been inferred to be associated with edifice collapse, landslide, and pyroclastic flow events for a variety of volcanic systems (Ward and Day, 2001; Watts and Waythomas, 2003), observation of such phenomena is rare. Inspection of nearshore deposits (scattered logs and fishnet floats) implied wave splash runups to heights of ~21 m above mean sea level (amsl) on the south flank of the fan at White's Bottom Ghaut (near b in Fig. 1). An 8.5 m amsl strandline of moderately concentrated flotsam (logs, coconuts) occurred on the east part of the fan, and is interpreted as recording the passage of several similarly high wave runups. Farther north (3.3 km from TRF), a densely concentrated accumulation of logs and mixed flotsam occurred at a maximum height of 6.8 m amsl at the southeast edge of Spanish Point (near c in Fig. 1).

The recognition of tsunami-related strandlines is unclear north of Spanish Point; however, the White's Bottom Fan was formed from PF deposition on 8 December 2002, and any loose debris available for reworking there was sparse. This accounts for lesser concentrations of flotsam here, and for its unambiguous interpretation. Wave runup strandlines on Montserrat, therefore, decrease systematically from TRF toward Trant's Bay, an observation consistent with tsunami rather than storm surge generation. In addition, there were no major hurricanes to cause high storm surge on Montserrat in the 3 yr prior to the 2003 collapse.

On Guadeloupe, 50 km SSE of Montserrat, a field survey of the western coast was conducted in November 2003 (Fig. 1). The survey team concluded that a tsunami occurred with a wave height of ~50 cm, which they attributed to the Soufrière Hills volcano collapse (Pelinovsky et al., 2004).

SEISMIC AND STRAIN OBSERVATIONS

Next we concentrate on the dilatometer signals for 12–13 July 2003 (Fig. 2). After 22:00, a curious oscillatory strain signal appears on all three
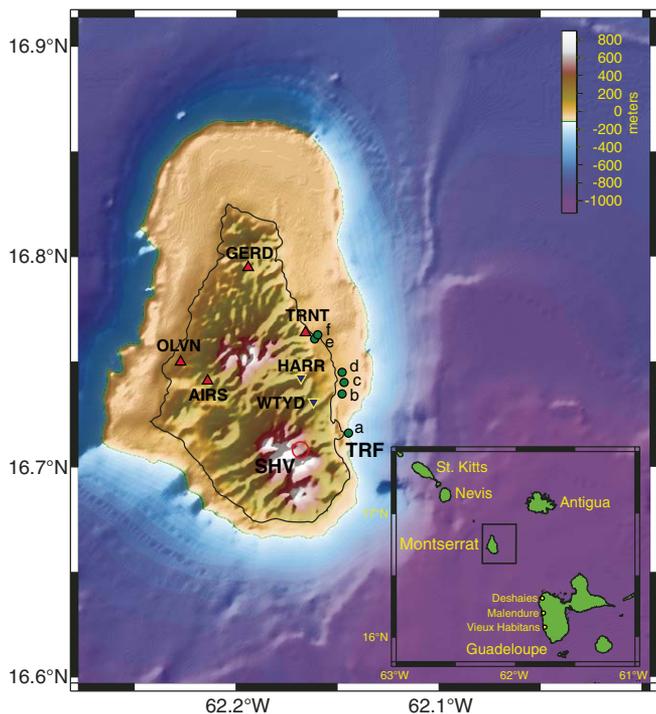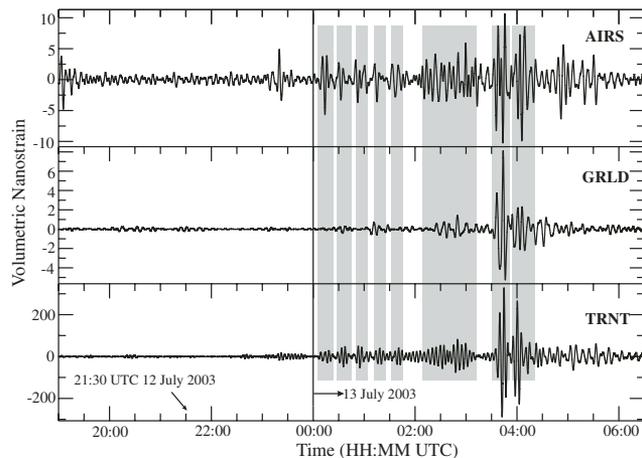
Figure 1. Regional map (inset) and computational grid for tsunami simulations. Topography and bathymetry are resampled to 50 m. CALIPSO borehole sites (AIRS, OLVN, GERD, and TRNT) are upright red triangles, and Harris (HARR) surface broadband seismic station and White's Yard camera and continuous global positioning system (cGPS) site are inverted blue triangles (WTYD). Numerical wave gauges, time series of which are shown in Figure DR1 (see text footnote 1), are green circles. Lava dome of July 2003 at Soufrière Hills Volcano (SHV) is red open circle, and Tar River Fan, where dome-collapse pyroclastic flows entered sea, is labeled TRF.

Figure 2. Strainmeter time series at AIRS, GERD, and TRNT. Records start at 19:00 (UTC) 12 July 2003. Data were acquired at 50 Hz using 16 bit A/D Reftek data acquisition system and were bandpass-filtered from 250 to 500 s to remove tidal and other effects. Note correlated structure of each site's signal. Earliest evidence of strain energy is seen clearly in AIRS and TRNT traces at ~20:00 12 July, and maximum amplitude signal on all three traces occurs at ~03:30 13 July 2003. Dominant period in all three dilatometer traces is 300 ± 100 s.

dilatometers; it is intermittent and occurs in unevenly spaced packets of several wavelengths duration, with larger amplitude signals occurring later in the sequence. The signal amplitude is ~40 times larger at TRNT than at the other two stations. Individual packets are well correlated between the three stations, although individual wavelets fall in and out of phase. The dominant period is ~300 ± 100 s. Periods for the TRNT dilatometer are illustrated using a spectrogram and are 200–250 s for collapse part I, 150–300 s for part II, 100–500 s for part III (peak), and 200–500 s for part IV (Fig. 3). High-frequency (~2–8 Hz) seismic packets associated with pulses of dome collapse lead the 300 s strain signal packets by 7–10 min. The temporal variation in strain period indicates a change in wave character during the evolution of the collapse, probably reflecting source conditions. Maximum seismic amplitude occurred in collapse part IIIa, corresponding to a maximum strain amplitude of ~325 nanostrain, when bandpass-filtered between 0.002–0.004 Hz, that increases to ~800 nanostrain at 0.0045 Hz (Fig. 3F), if unfiltered. The strain wave packets at GERD and AIRS, while much smaller in amplitude, lead the corresponding wave packet at TRNT by 2–3 min.

We infer that these observations are consistent with a secondary source rather than one arising from deep magmatic processes, and the obvious candidate involves tsunamis generated by PFs entering the ocean at TRF. To test our hypothesis, we reconstructed the prolonged collapse from seismic data (Calder et al., 2002; Norris, 1994) to establish constraints on volumes and other characteristics of the flowing debris, which served as wavemakers. The continuous broadband seismic record at HARR was used to reconstruct the developing lava dome collapse on 12 July. Seismic energy related to PFs is mainly high frequency, so we filtered data at 3 Hz to remove spurious long-period energy (Miller et al., 1998).

The amplitude of the >3 Hz signal (Fig. 3A) reveals that the collapse was neither continuous nor uniform; PFs were generated instead in dis-

crete packets, the amplitudes of which tended to increase as the collapse progressed toward its climax. The integrated envelope of signal amplitude at HARR is assumed as a proxy for total PF volume (Brodscholl et al., 2000); the area bounding individual peaks on the amplitude plot then gives an estimate of volume for individual events. Our method assumes that the PFs originate at a common source and follow the same track, which is reasonable given the descent of all flows in the Tar River valley. Figure 3 (A–D) compares the volumetric strain with the seismic vertical-component at HARR, and shows clearly the strain signals for cluster I, with increasing amplitudes in cluster II through dome collapse clusters IIIa and IIIb (GSA Data Repository Table DR1[1]).

TSUNAMI GENERATION AND PROPAGATION MODELS

We infer that the dense base of a PF forms a coherent tsunami in the near field, or just beyond where the material decelerates strongly under the water. We construct our tsunami sources by applying the tsunami amplitude η_0 and wavelength λ_0 (Walder et al., 2003) within the Tsunami Open and Progressive Initial Conditions System (TOPICS) (Grilli and Watts, 1999). We use a simple model for basal PF mass motion (Watts and Waythomas, 2003), which is based on detailed studies of the complex behavior of debris flows (Iverson and Denlinger, 2001; Savage and Hutter, 1989). TOPICS outputs a complete ocean surface initial condition used in a tsunami propagation model.

Like a pebble tossed in a pond, a PF penetrating the ocean will generate continuous arcs of wave fronts. To simulate different water wave physics along the TRF front as a function of local water depth, we subdivided the PF entry arc into subsections (Watts and Waythomas, 2003): two subsections in shallow water on either side of the entry position generate edge waves, two subsections in deeper water generate wave components at some acute angle on either side of the axis of debris flow (transformed from a PF) motion, and one subsection creates wave components along the centerline of debris-flow motion, beyond where the material stalls underwater. Complete inputs and selected outputs from TOPICS are provided in Table DR2 (see footnote 1).
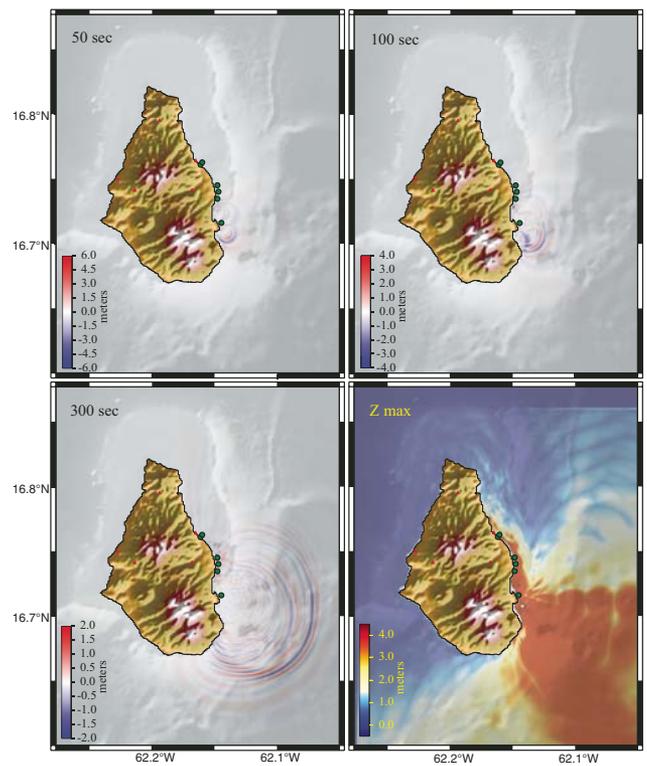
For wave propagation we use the nonlinear Boussinesq model Geowave, designed to model the fluid mechanics of breaking waves and

---

[1]GSA Data Repository item 2007015, Table DR1 (detailed reconstruction of dome collapse events), Table DR2 (summary of TOPICS inputs for PF sources), and Figure DR1 (numerical wave gauges for tsunami simulation shown in Fig. 4), is available online at www.geosociety.org/pubs/ft2007.htm, or on request from editing@geosociety.org or Documents Secretary, GSA, P.O. Box 9140, Boulder, CO 80301, USA.
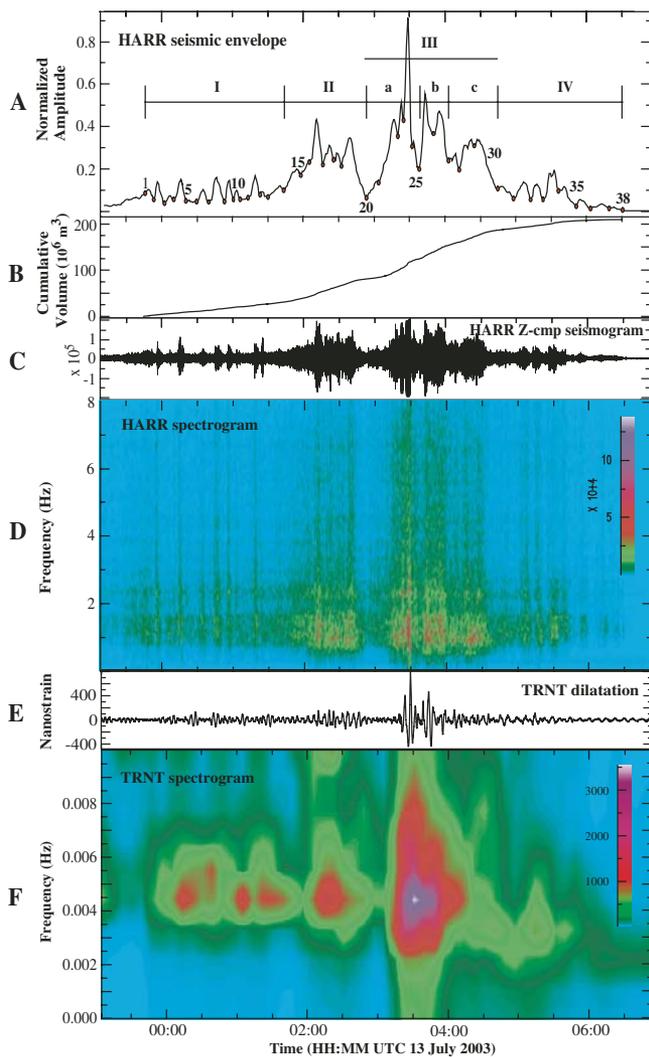
Figure 3. A: Normalized seismic amplitude for HARR surface broadband seismometer. All records start at 23:00 (UTC) 12 July 2003. Individual pyroclastic flows are annotated on seismic envelope and major divisions are shown as Roman numerals. B: Cumulative collapse volume from HARR-normalized amplitude in A. C: HARR vertical component seismogram. D: Spectrogram for seismogram in C. Note that most of power is in 1–3 Hz band and that higher frequency energy is observed during significant collapse events. E: TRNT dilatation highpass filtered at >0.002 Hz. Peak amplitudes in dilatation that occur 7–10 min after same events are recorded as seismic energy at HARR. F: Spectrogram for TRNT dilatation in E. Most of power is between 0.004 and 0.006 Hz, and during peak collapse event III, energy is spread to higher frequencies.

Figure 4. Geowave simulations at 50–300 s. Colors (red for wave heights above, and blue for wave heights below, sea level) are scaled to model extremes. Simulations are for 7 Mm³ pyroclastic flow entering sea at ~70 ms⁻¹ with volume-to-width ratio of 16700 m². Z max is maximum wave height over entire temporal domain. Eastern Montserrat, from TRF to Trant's Bay, experienced maximum waves of few meters, with heights as high as 14 m localized proximal to TRF.

to simulate inundation (Wei and Kirby, 1995; Chen et al., 2000). Geowave has been validated for several underwater landslide- and debris-flow–generated tsunamis (Watts et al., 2003; Walder et al., 2003). In Figure 4, tsunami wave fronts are illustrated at times between 50 and 300 s for a source volume of $\sim 7 \times 10^6$ m³ and a nominal entry velocity ~70 m/s. These conditions were selected to be broadly representative of PFs entering the sea at the TRF during the collapse at Soufrière Hills volcano and, while not depicting the most extreme event, are within the bounds inferred by direct observation and detailed analysis of seismic amplitudes (Herd et al., 2005). At 50 s, the frontal arc has reached the White's Bottom Fan and the frontal arc has wrapped around the fan at Spanish Point to meet with a refracted wave front striking due north, whereas closer to the source, the wave interference pattern reflects the dual edge sources. It is difficult to resolve these waves from the deep-water sources, which are smaller in amplitude; the edge waves from the impact zone dominate the wave

patterns (Fig. 4). By 100 s, the first waves approach Trant's Bay, although these initial waves are smaller than others in the wave train.

The model wave train may be examined in the temporal domain by numerical wave gauges at selected points within the computational grid (Fig. 1; Fig. DR1). Waves with heights of ~1.2 m appear after ~600 s at Trant's Bay (Fig. 4 and gauges e and f; Fig. DR1); nearshore gauges display complexities from wave interference, and spatial integration was used to average these effects in order to estimate the loads sensed by the TRNT dilatometer (Fig. 2). The maximum wave heights averaged for semicircular arrays at 250 and 500 m offshore, respectively, are 0.52 and 0.22 m.

OCEAN LOADING MODELS AND COMPARISON WITH STRAIN

We developed a simple model of ocean loading at TRNT, where the ocean load change is taken as a slab of water of uniform height, terminating at the shoreline. Sensor depth is close to the edge of the ocean load (180 m deep and 40 m horizontally inland), relative to the wavelength of the tsunami (380 m). For a water wave amplitude of 1 m, $P = 10$ kPa, and the mean stress at the dilatometer, σ_m, is ~3.6 kPa (Poulos and Davis, 1974). Volumetric strain $(\varepsilon_v) = \sigma_m/K = 3\,\sigma_m\,(1 - \upsilon)/E \sim 3\,\sigma_m/2E$, where K and E are bulk and Young's moduli, respectively, and υ is Poisson's ratio. Taking E to be ~10 GPa (based on dilatometer calibrations), we estimate $\varepsilon_v = 0.54$ µε/m of wave height, which decreases to 0.25 µε/m if the edge of the load is assumed to be 250 m away.

The peak amplitude of the observed strain signal at TRNT (~0.32 µε) at 03:30 13 July 2003 is thus consistent with loading by a tsunami of ~0.6 m (40 m horizontal distance) to ~1.3 m (250 m horizontal distance) height from our static loading model. Expected wave heights would increase to 1.5–3.2 m, if peak strain amplitude is ~0.8 µε. Our simulation yields wave heights of 0.2–0.5 m for spatial averages at 500 and 250 m radial arcs, and yields 0.5–1.2 m for individual gauges f and e, respectively (Fig. 1; Fig. DR1 [see footnote 1]);

these wave heights derive from an inferred near-source tsunami wave of ~1.2 m height immediately north of the TRF (gauge a in Fig. 1; Fig. DR1).

Model tsunami heights are too low in all cases to account for the maximum strain amplitude. This either implies that significantly more energetic PFs (or larger volume, if velocity is held constant) than those simulated would have occurred during the peak collapse event of IIIa (Fig. 3A), or that the simple block model may not generate appropriate initial conditions for a given volume. Wave runup is generally ~2–4 times higher than the offshore wave heights (Watts and Waythomas, 2003; Synolakis, 1987). At the eastern end of White's Bottom Ghaut and Spanish Point (gauges b and d in Fig. 1; Fig. DR1), however, our simulation yields values that are between 53% and 93% of the observed runup features. We infer that larger masses were probably involved in producing the largest tsunami and maximum runup and that the highest runup observed at Whites Bottom fan likely reflects splash-zone effects, rather than coherent wave propagation (Watts and Waythomas, 2003).

In the near field, edge waves produced the highest runups. The majority of the water wave energy is directed southeast, but that wave front is dissipated peripherally. Within several additional minutes, water waves reached Trant's Bay and a large ocean-loading strain signal was recorded on the TRNT dilatometer. Subsequent tsunamis for an individual PF-generated packet impacted the coastline at intervals of ~300 s, 3–5 waves being recorded for each collapse event. The time delay between PF generation, as recorded on the seismometer, and ocean loading, as recorded on the dilatometer, is consistent with dispersal times for a tsunami wave generated at TRF and moving northward to Trant's Bay and the TRNT borehole. Further, the modeled wavelength of a tsunami generated by each PF packet is consistent with the period of the strain signal (~300 s).

In summary, tsunamis were generated by each PF entering the ocean at TRF, with initial wave heights directly related to the volume of individual PF packets. The first oceanic impacts of debris (and steam explosions) generated a volumetric strain signal initially recorded at AIRS and GERS as a result of direct elastic wave transmission; this occurred a few minutes after peak PF energy release occurred on the runout track, which explains the observations of elastic wave arrivals at AIRS and GERS prior to the larger-amplitude water-wave arrivals at TRNT.

CONCLUSIONS

Tsunamis generated by PFs have been recorded sparsely, mainly from tide marks on the shoreline on Montserrat (Young et al., 2002), or from onshore deposits in Alaska (Waythomas and Neal, 1998), but never by such sophisticated geophysical instruments as CALIPSO.

Our results are qualitatively similar to those of Heinrich et al. (1998) for a hypothetical 40 Mm³ collapse and tsunami event at TRF. In that model, the slide mass was allowed to fall as a single body, resulting in greater initial wave heights. In our analysis, however, we have tied individual, moderate-sized PFs with ocean surface excitation and wave propagation.

Tsunami generation at island or lakeside volcanoes is far more common than the historical record and/or scientific literature indicate, and thus we conclude that any volcano within a few kilometers of water and capable of generating hot pyroclastic flows or cold debris flows with volumes in excess of 5×10^6 m³ has the potential to generate significant and possibly damaging tsunamis during a future eruption.

REFERENCES CITED

Brodscholl, A., Kirbani, S.B., and Voight, B., 2000, Sequential dome-collapse nuees ardentes analyzed from broadband seismic data, Merapi Volcano, Indonesia: Journal of Volcanology and Geothermal Research, v. 100, p. 363–369.

Calder, E.S., Luckett, R., Sparks, R.S.J., and Voight, B., 2002, Mechanisms of lava dome instability and generation of rockfalls and pyroclastic flows at Soufrière Hills Volcano, Montserrat, in Druitt, T.H. and Kokelaar, B.P., eds., The eruption of Soufrière Hills volcano, Montserrat, from 1995 to 1999: Geological Society [London] Memoir 21, p. 173–190.

Chen, Q., Kirby, J.T., Dalrymple, R.A., Kennedy, A.B., and Chawla, A., 2000, Boussinesq modeling of wave transformation, breaking, and runup. II: 2D: Journal of Waterway, Port, Coastal, and Ocean Engineering, v. 126, p. 48–56.

Druitt, T.H., and Kokelaar, B.P., 2002, The eruption of Soufrière Hills Volcano, Montserrat, from 1995 to 1999: Geological Society [London] Memoir 21, p. 645.

Edmonds, M., and Herd, R.A., 2005, Inland-directed base surge generated by the explosive interaction of pyroclastic flows and seawater at Soufriere Hills Volcano, Montserrat: Geology, v. 33, p. 245–248.

Grilli, S.T., and Watts, P., 1999, Modeling of waves generated by a moving submerged body. Applications to underwater landslides: Engineering Analysis with Boundary Elements, v. 23, p. 645–656.

Heinrich, P., Mangeney, A., Guibourg, S., Roche, R., Boudon, G., and Cheminee, J.-L., 1998, Simulation of water waves generated by a potential debris avalanche in Montserrat, Lesser Antilles: Geophysical Research Letters, v. 25, p. 3697–3700.

Herd, R.A., Edmonds, M., and Bass, V.A., 2005, Catastrophic lava dome failure at Soufrière Hills Volcano, Montserrat, 12–13 July 2003: Journal of Volcanology and Geothermal Research, v. 148, p. 234–252.

Iverson, R.M., and Denlinger, R.P., 2001, Flow of variably fluidized granular masses across three-dimensional terrain; 1, Coulomb mixture theory: Journal of Geophysical Research, B, Solid Earth and Planets, v. 107, p. 537–552.

Mattioli, G.S., Young, S.R., Voight, B., Steven, R., Sparks, J., Shalev, E., Malin, P., Linde, A., Johnson, W., Hidayat, D., Elsworth, D., Dunkley, P., Herd, R., Neuberg, J., Norton, G., and Widiwijayanti, C., 2004, Prototype PBO instrumentation of CALIPSO Project captures world-record lava dome collapse on Montserrat Volcano: Eos (Transactions, American Geophysical Union), v. 85, p. 317–325.

Miller, A.D., Stewart, R.C., White, R.A., Luckett, R., Baptie, B.J., Aspinall, W.P., Latchman, J.L., Lynch, L.L., and Voight, B., 1998, Seismicity associated with dome growth and collapse at the Soufrière Hills Volcano, Montserrat: Geophysical Research Letters, v. 25, p. 3401–3404.

Norris, R.D., 1994, Seismicity of rockfalls and avalanches at three Cascade Range volcanoes; implications for seismic detection of hazardous mass movements: Seismological Society of America Bulletin, v. 84, p. 1925–1939.

Pelinovsky, E., Zahibo, N., Dunkley, P., Edmonds, M., Herd, R., Talipova, T., Kozelkov, A., and Nikolkina, I., 2004, Tsunami generated by the volcano eruption on July 12–13, 2003 at Montserrat, Lesser Antilles: Science of Tsunami Hazards, v. 22, p. 44–57.

Poulos, H.G., and Davis, E.H., 1974, Elastic solutions for soil and rock mechanics: New York, John Wiley & Sons, 411 p.

Savage, S.B., and Hutter, K., 1989, The motion of a finite mass of granular material down a rough incline: Journal of Fluid Mechanics, v. 199, p. 177–215.

Synolakis, C., 1987, The runup of solitary waves: Journal of Fluid Mechanics, v. 185, p. 523–545.

Walder, J.S., Watts, P., Soresen, O.E., and Janssen, K., 2003, Tsunamis generated by subaerial mass flows: Journal of Geophysical Research, B, Solid Earth and Planets, v. 108, p. 2236.

Ward, S.N., and Day, S., 2001, Cumbre Vieja Volcano; potential collapse and tsunami at La Palma, Canary Islands: Geophysical Research Letters, v. 28, p. 3397–3400.

Watts, P., and Waythomas, C.F., 2003, Theoretical analysis of tsunami generation by pyroclastic flows: Journal of Geophysical Research, B, Solid Earth and Planets, v. 108, p. 21.

Watts, P., Grilli, S.T., Kirby, J.T., Fryer, G.J., and Tappin, D.R., 2003, Landslide tsunami case studies using a Boussinesq model and a fully nonlinear tsunami generation model: Natural Hazards and Earth System Sciences, v. 3, p. 391–402.

Waythomas, C.F., and Neal, C.A., 1998, Tsunami generation by pyroclastic flow during the 3500-year B.P. caldera-forming eruption of Aniakchak Volcano, Alaska: Bulletin of Volcanology, v. 60, p. 110–124.

Wei, G., and Kirby, J.T., 1995, Time-dependent numerical code for extended Boussinesq equations: Journal of Waterway, Port, Coastal, and Ocean Engineering, v. 121, p. 251–261.

Young, S.R., Voight, B., Barclay, J., Herd, R.A., Komorowski, J.C., Miller, A.D., Sparks, R.S.J., and Stewart, R.C., 2002, Hazard implications of small-scale edifice instability and sector collapse; a case history from Soufrière Hills Volcano, Montserrat, in Druitt, T.H. and Kokelaar, B.P., eds., The eruption of Soufrière Hills volcano, Montserrat, from 1995 to 1999: Geological Society [London] Memoir 21, p. 349–461.